Variations of Winds and Turbulence Seen by the 50-MHz Radar at White Sands Missile Range, New Mexico

G. D. NASTROM

St. Cloud State University, St. Cloud, Minnesota

F. D. EATON

Army Research Laboratory, White Sands Missile Range, New Mexico

(Manuscript received 7 February 1995, in final form 12 April 1995)

ABSTRACT

The mean vertical profiles of the winds from about 5 to 20 km at White Sands Missile Range, New Mexico, are described. The variability of wind speed, spectral width, volume reflectivity calibrated as C_N^2, and vertical wind shear are documented as functions of season and of time of day using observations taken from 1991 through April 1994 with the 50-MHz profiling radar. The mean meridional winds are from the south at about 1–3 m s^{-1} during every season except autumn, and mean zonal winds have a broad jet near the tropopause with maximum speed over 30 m s^{-1} during the winter. The mean vertical velocity is downward at about 5 cm s^{-1} in the troposphere and is weakly upward in the lower stratosphere. The shear of the mean wind and the mean wind shear have small interseasonal variability. The variance over 1-h periods of all three wind components, the spectral width, and C_N^2 have lognormal frequency distributions. The variance of the meridional wind speed is greater than that of the zonal wind speed in the troposphere, but in the stratosphere during winter and spring the variance of the zonal wind speed is greater. The mean profiles of $\log C_N^2$ in the stratosphere are nearly constant with altitude and from season to season, ranging over only a few decibels. Diurnal cycles of wind speed have amplitudes on the order of 1 m s^{-1}, but the phases are highly variable with height and season, suggesting strong local topographic control of the observed diurnal cycles. The diurnal cycles of C_N^2, spectral width, and of the variance of the vertical velocity have the largest amplitudes in the troposphere where the daily maxima are during the afternoon.

1. Introduction

Mesosphere–stratosphere–troposphere (MST) radars, also known as wind profilers, can observe the atmospheric winds and turbulence with relatively high time and space resolution. A recent review of MST radar principles, capabilities, and applications has been given by Gage (1990). A 50-MHz radar with very large power aperture product (10^8 W m^2) has been operated at White Sands Missile Range (WSMR), New Mexico, since January 1991. Over three years of nearly continuous data are now available. The purpose of this paper is to describe the mean vertical profiles of the winds and turbulence and their variability with season and time of day at WSMR using this dataset.

The WSMR radar observations have high time and vertical resolution and are relatively continuous in time, making this dataset unique among large radars. Its vertical resolution is 150 m, rather than 2 km as used at Poker Flat, Alaska (Balsley et al. 1979). It is operated in a monitoring mode, rather than in a campaign mode as used at most other radars with large power aperture products, such as the middle and upper atmosphere (MU) radar (Kato et al. 1986) and the SOUSY radar (Ruster et al. 1986). A radar identical to the WSMR 50-MHz radar, except that the WSMR system is calibrated for C_N^2, is operated at Cape Kennedy in support of space shuttle launches (Wilfong et al. 1993).

Our paper is organized as follows. Section 2 describes the observing site and available data. Section 3 discusses the seasonal means of wind speed, vertical wind shear, the refractivity turbulence structure constant, C_N^2, and spectral width, along with indications of interannual variations of these variables. Diurnal variations are presented in section 4, and our concluding remarks are given in section 5.

Corresponding author address: Dr. Gregory D. Nastrom, Department of Earth Sciences, St. Cloud State University, 720 Fourth Avenue South, St. Cloud, MN 56301-4498.
E-mail: NASTROM@TIGGER.STCLOUD.MSUS.EDU

2. Observing site and available data

The 50-MHz radar used in this study is one of four radar systems operating at the Atmospheric Profiler

Research Facility (APRF) at WSMR. In addition is a 404-MHz radar (part of the National Oceanographic and Atmospheric Administration Wind Profiler Demonstration Network), a 924-MHz boundary layer profiler, and an FM-CW radar. A radio acoustic sounding system was added to the 50-MHz radar system in mid-1992. It uses three acoustic sources, each transmitting 1600 W of acoustic power, and commonly derives temperature profiles to 11 km with occasional profiles to 15 km. A more complete description of all equipment at the APRF, including optical devices, sodar, instrumented towers, and a radiation station, is given by Hines et al. (1993). Details of the FM-CW radar and examples of its data are given by Eaton et al. (1995). For some analyses it is necessary to use data from multiple observing systems; however, the goal of this study is to document the variability of the winds and turbulence as seen by the 50-MHz radar.

The APRF is located in the Tularosa Basin at 32°24′N, 106°21′W (about 10 km east of the headquarters area of WSMR) at 1220 m above sea level. While the immediate site is relatively flat and covered by mesquite, etc., indigenous to the Chihuahuan Desert, the San Andres and Organ Mountains run north–south and are located west of the APRF. Organ Peak (2704 m MSL) is 13 km southwest of the APRF. These mountains are steep and create a physical "knife edge" affecting eastward airflow. The Sacramento Mountains, also running north–south, lie about 30 km east of the APRF.

TABLE 1. Radar parameters used in this study.

Transmitter	
Nominal frequency	49.25 MHz
Output power	250 kW peak
Duty cycle	5%
Pulse width (compressed)	8 μs (8:1) 1 μs nominal
Type	Combination solid-state preamplifier and tube-cavity amplifier, three stage
Antenna	
Physical aperture	15 600 m^2
Effective aperture	13 500 m^2
Pointing	Zenith and 15° to north and east
Type	Coaxial-collinear phased array
One-way beamwidth	2.9°
Receiver	
Type	Low-noise superheterodyne
Bandwidth	Matched to transmitted pulse
Receiver noise figure	Less than 1 dB
Performance	
Nominal lowest range gate	2 km above ground level
Range gate spacing	150 m
Time resolution	1 min per beam
Number of range gates	112
Horizontal wind range	$\pm$116 m s^{-1}
Calibrated C_N^2 range	10^{-20}–10^{-13} m$^{-2/3}$
Bandwidth	1 MHz
Power aperture product	1×10^8 W m^2

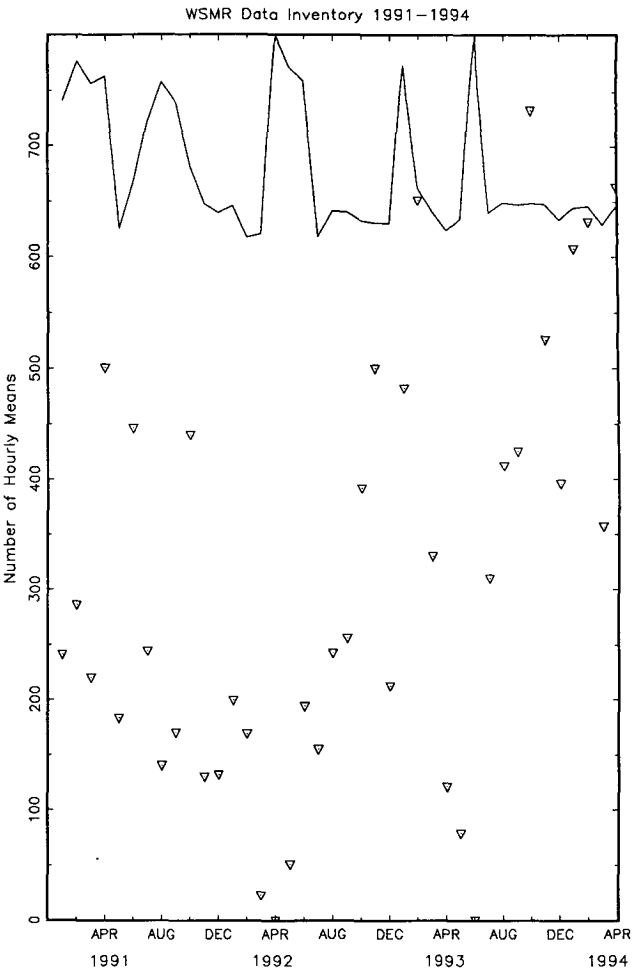

FIG. 1. Monthly inventory of the data available at WSMR during January 1991–April 1994. Triangles show the number of hourly means during each month, and the solid line shows the average number of observations during each hour with 20 observations corresponding to full scale. Stippled area denotes times when data were available only during night hours.

Climatological records of surface observations at the APRF do not exist. Temperature, wind, and cloud-cover records taken at other sites at WSMR (e.g., Hoidale et al. 1975) are not necessarily transferable to the APRF because of local terrain effects; for example, in the summer during early afternoon cumulus clouds commonly form over the mountains east and west of the APRF, and later in the day drift over the Tularosa Basin.

The operating parameters of the 50-MHz radar at WSMR are given in Table 1. The radar has three beams

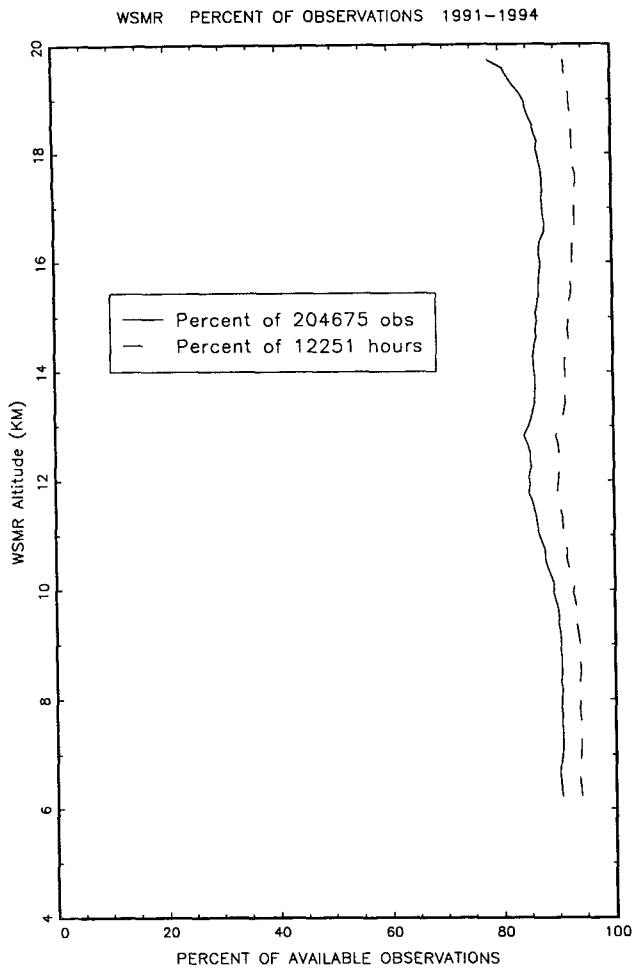

FIG. 2. The percent of observations and hourly means available on the east–west oblique beam as a function of altitude above mean sea level (only hours with five or more profiles were retained for analysis).

(north, east, and vertical) and each beam is sampled for 1 min in a continuous rotation, providing vertical profiles with 150-m resolution from about 6 to 20 km MSL every 3 min. Data used here consisted of complete profiles of the first three moments of each Doppler spectrum: mean Doppler velocity, spectral width, and returned power reported as C_N^2 through calibration by internal comparisons against a known noise source, as explained by Hines et al. (1993) and references therein. All analyses reported here were made using hourly mean values of the data that survived quality control checks. Problems with the radar system electronics rendered the data below about 6 km useless. Other details of the radar design and operation, along with examples of the data, a discussion of data quality control procedures, and case studies of the relationships of winds, turbulence, and weather are given by Nastrom and Eaton (1993a,b).

The basic period of record available for this study was January 1991–April 1994. Generally, the radar operated continuously. However, inspection of monthly height–time plots of the hourly means of the moments revealed that the radar operated only 6 h per day (during the night) from 27 October 1991 through 2 June 1992; therefore these months will not be used in studies of diurnal variations. It was also noted that some brief periods, especially January–March 1994, had anomalously low C_N^2 values, suggesting a calibration problem, and thus only wind values were used during these periods.

The number of hours of observations available for each month are given in Fig. 1, along with the average number of profiles available each hour. Typically, about 16 profiles are available each hour. There is no obvious trend with time in the number of data available. During this period, data for 204 675 individual profiles were collected during a total of 12 251 h. The profile of the percent of total data available that passed all quality control checks for the oblique beam in the east–west plane is given in Fig. 2. An hourly mean at a given height was retained for further analysis only if it was based on 5 or more observations. Over 90% of the hours had useful means at all altitudes as shown in Fig. 2.

3. Seasonal and interannual variations

a. Horizontal winds

Figure 3 shows the mean profiles of zonal (u) and meridional (v) winds as functions of season (winter is December, January, February, etc.). The number of hourly means used at 7 km is given by N for each season. Mean meridional winds are relatively light at all altitudes and are from the south during all seasons except fall and, above about 17 km, during winter. Mean zonal winds are from the west except above 17 km during the summer when the WSMR radar observations reach into the stratospheric easterlies. The maximum wind speed, the jet, is strongest during winter when the nose of the jet in the mean winds is relatively uniform at nearly 32 m s^{-1} from about 10 to 13 km. The jet on any given day may be much stronger than the mean, but often it is confined in vertical extent to a region near the tropopause. The flat nose of the mean jet partially results from the large vertical excursions of the daily jets associated with changes in tropopause height during passing baroclinic systems. However, it should be noted that the jet on individual radar profiles sometimes has a flat nose, presumably because turbulence is very low in the center of the jet, and thus radar echoes are weak in the center of the jet and have unacceptably low signal-to-noise values there (see, e.g., Weber et al. 1990).

Seasonal means of the winds observed by twice-daily rawinsondes over the same period at El Paso, about

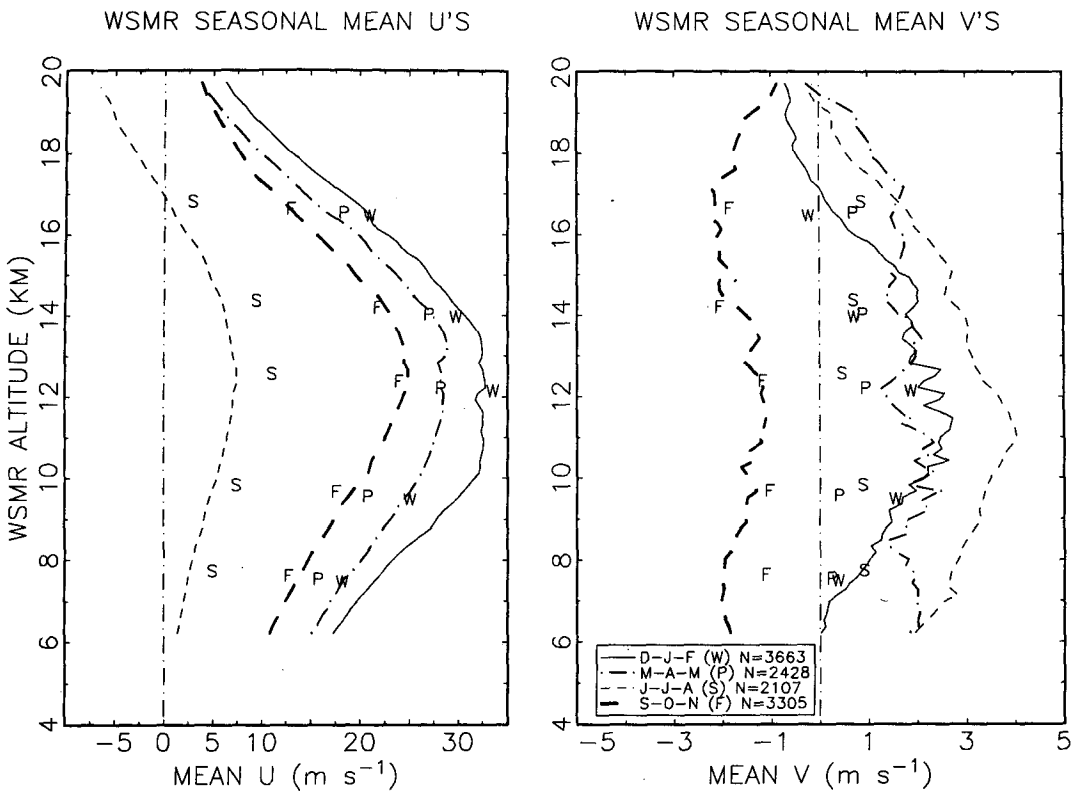

FIG. 3. Seasonal mean zonal (left) and meridional (right) winds at WSMR for January 1991–April 1994. Small letters show the means from twice-daily rawinsonde flights at El Paso.

50 km south of WSMR, have been added in Fig. 3 for comparison. About 500 balloon profiles were used each season. Comparison of the balloon and radar wind profiles shows that the balloons capture the gross features of the mean wind profile. Many of the small differences between the balloon and radar profiles may be attributed to the difference in location. However, some of the differences, such as those in both wind components at all heights during summer, appear large and may be due to a bias in the balloon data due to

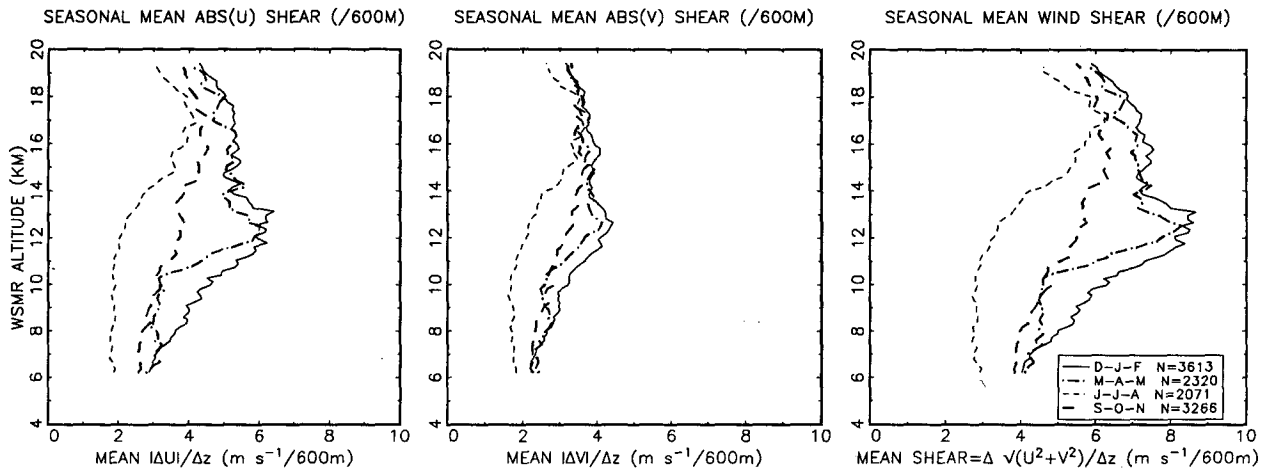

FIG. 4. Seasonal means of the vertical shear of the horizontal wind across 600-m layers.

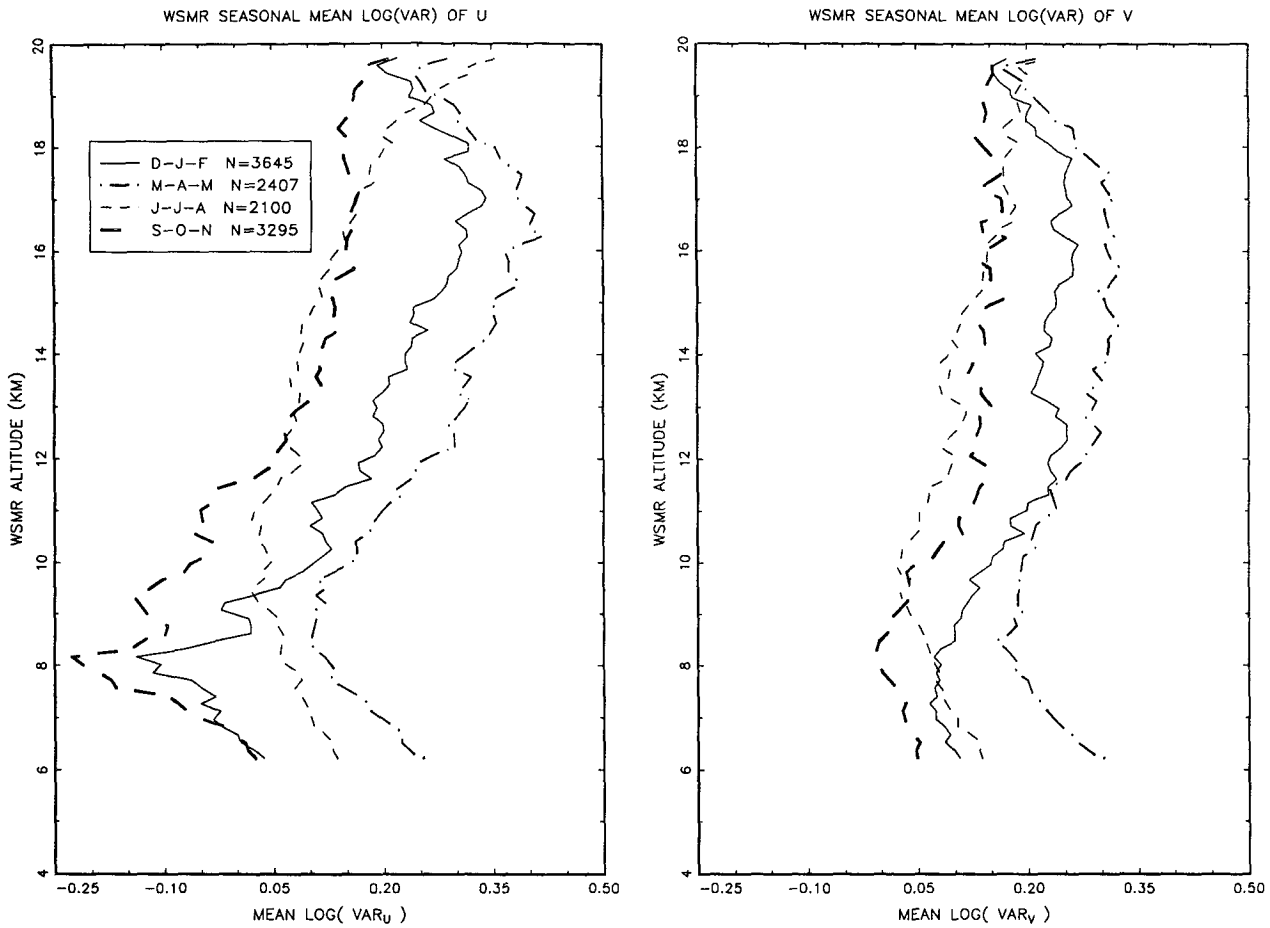

FIG. 5. Seasonal means of the variance ($m^2 s^{-2}$) of the zonal (left) and meridional (right) wind speeds over 1-h intervals.

the diurnal wind tide. Examples of analyses of the diurnal tides in winds and turbulence will be presented below, along with comparisons of the present results with past studies of diurnal tides. The point here is that continuous sampling with the wind profiler gives unbiased estimates of the daily mean wind while twice-daily rawinsondes may not.

The seasonal mean profiles of zonal wind in Fig. 3 have relatively similar shapes. Anticipating the discussion of C_N^2 and its dependence on vertical wind shear, note that except near the jet core the vertical shear of the mean wind is about the same during all seasons (except perhaps summer values have slightly less shear). The vertical wind shear at any given time may be very different from the shear of the mean winds implied by Fig. 3. Profiles of the seasonal means of the absolute values of the vertical shear of zonal and meridional winds and of the total shear, across 600-m layers and based on individual profiles, are compared in Fig. 4. Note that even for these mean shears the differences among seasons are relatively small at the upper altitudes and, except for summer, below about 11 km. Profiles of mean wind shear during winter and spring are nearly identical. Thus, since both the mean wind shear (Fig. 4) and the shear of the mean wind (Fig. 3) are similar among seasons, we might anticipate that seasonal mean profiles of C_N^2 will be similar if stability and humidity effects are similar.

Layers over 600 m are used in Fig. 4 in an effort to ensure that the atmospheric wind speed differences are greater than the uncertainty of the wind measurements. Estimates of the rms noise for radar horizontal winds are near 0.7 m s^{-1} at Kennedy Space Center, and thus also at WSMR (S. A. Smith 1994, personal communication), and therefore the noise limit for wind differences is about 1 m s^{-1}. The mean differences in Fig. 4 are all well above this limit. Mean differences based on smaller, 300-m layers (not shown), are nearly parallel to those in Fig. 4 and are reduced by a factor of about 2.

Figure 5 shows the seasonal mean profiles of the logarithm of the variances of the u and v winds over 1-h periods. Logarithms are used because the variances of all three wind components, u, v, and w, appear to

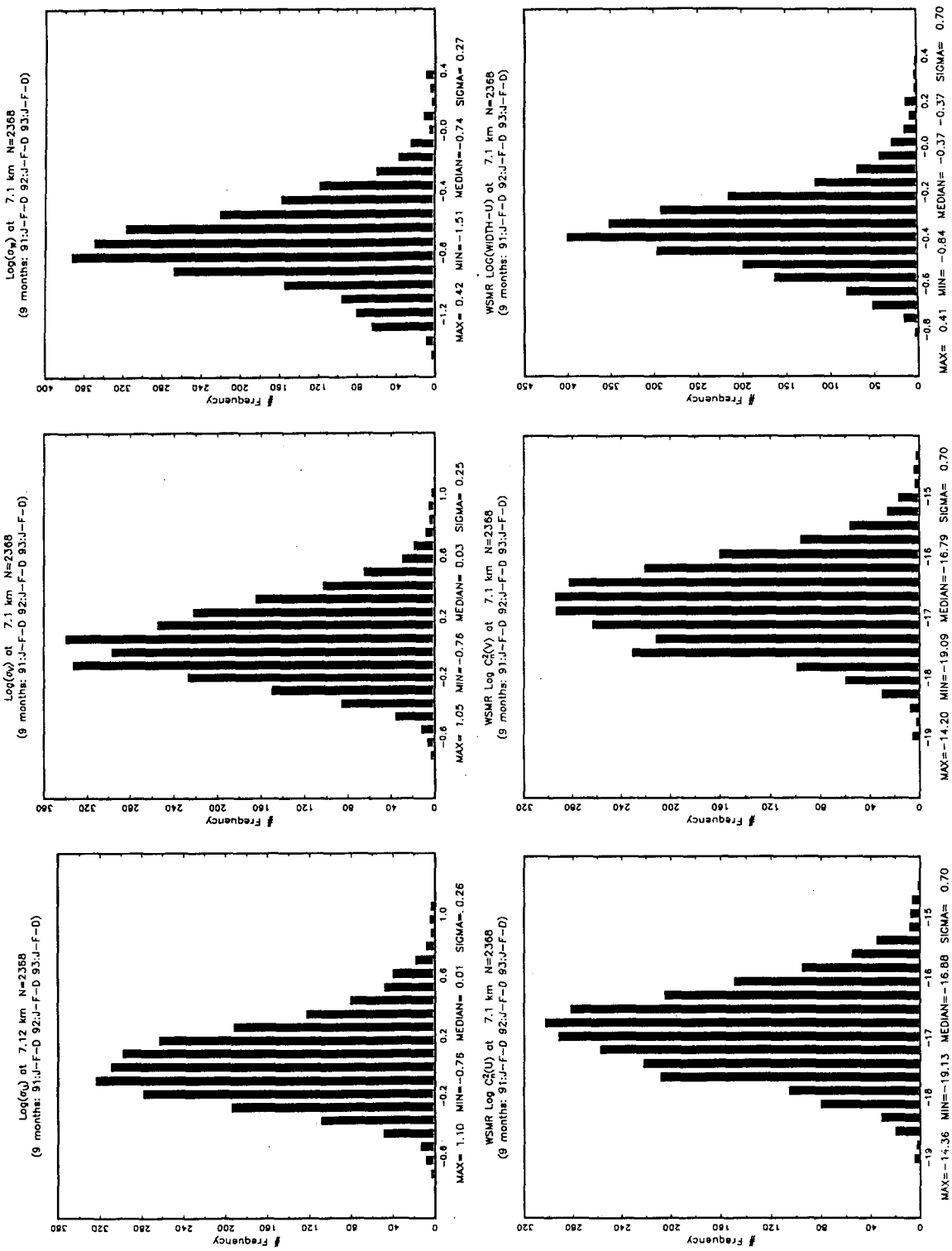

FIG. 6. Frequency distributions of the logarithm of the standard deviation (square root of the variance) of the components of the wind, the spectral width, and C_N^2 at WSMR during winter.

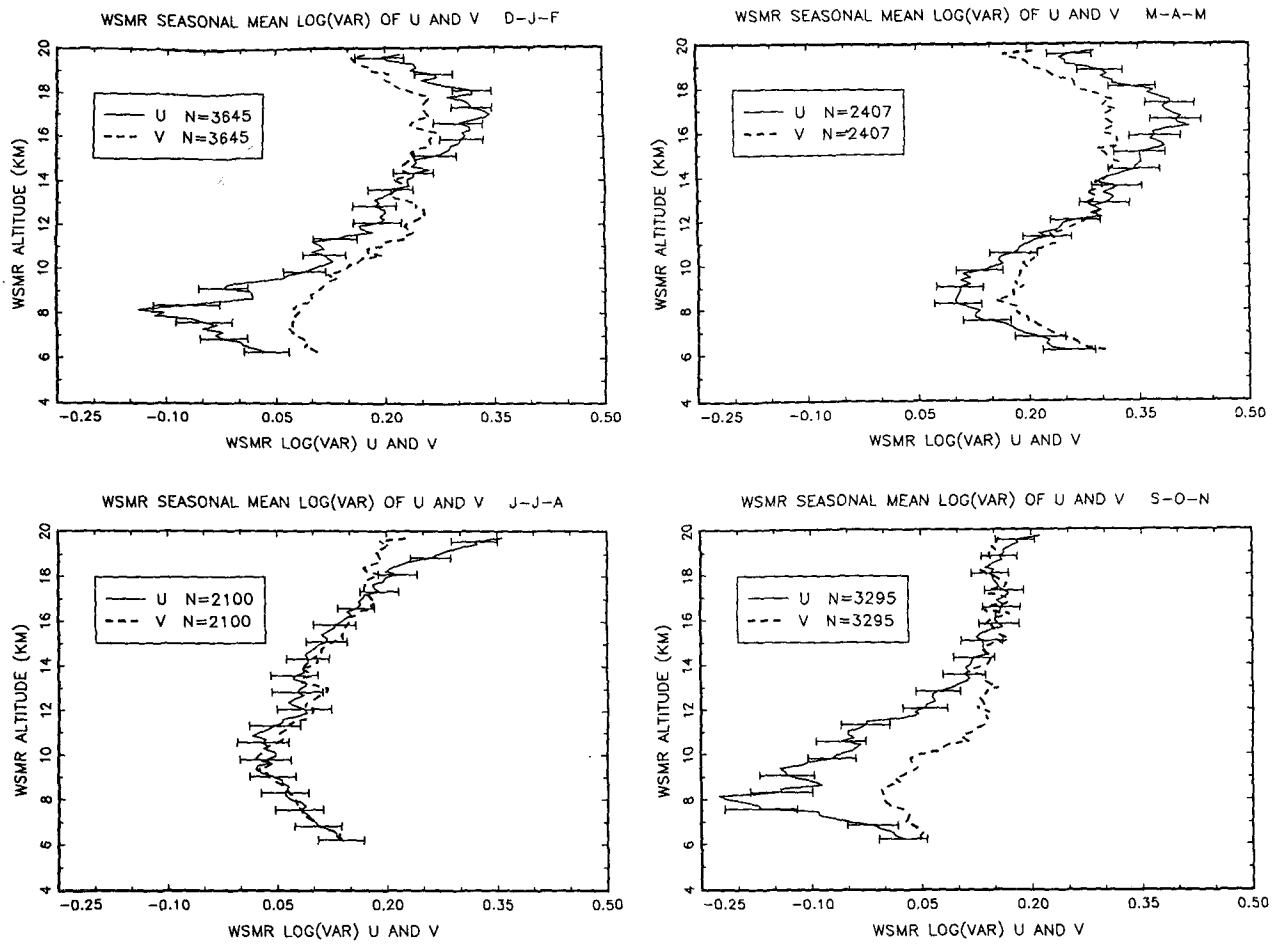

FIG. 7. As in Fig. 5 except comparing the zonal and meridional variance during each season.

have approximate lognormal frequency distributions as illustrated by the results for 7 km in Fig. 6. Frequency distributions at other levels (not shown) are similar (Nastrom 1995). Also, Fig. 6 shows that the frequency distributions of spectral width, related to the intensity of small-scale turbulence, and of C_N^2 are nearly lognormal. Returning to Fig. 5, the largest variances for both u and v are in spring near about 18 km, and the smallest variances are in autumn near about 8 km.

Isotropic processes will have equal variances in the u and v wind components. Figure 7 compares simultaneous seasonal profiles of the means of the logarithms of the 1-h variances of u and v to check for anisotropy. Error bars extend plus/minus one standard error of the mean from the mean, where SEM = $2\mathrm{SD}N^{-1/2}$ and SD is the standard deviation of the N values. During summer, when the flow is most likely controlled by local conditions, which are removed from the large-scale circulation, variances of u and v are similar at all altitudes below about 18 km. During all other seasons, the variance of the meridional wind is greater than that of the zonal wind in the troposphere ($\sigma_v^2 > \sigma_u^2$). In the stratosphere, however, $\sigma_v^2 < \sigma_u^2$, at least during winter and spring. The peak in the profile of $\sigma_v^2 + \sigma_u^2$ (not shown) is at about 17 km during winter and spring, and is above 20 km in summer and fall. The changes with azimuthal direction of the horizontal wind variances may be related to gravity wave propagation, although we can infer few details with observations at only two azimuths. VanZandt et al. (1990) conclude that azimuthal changes of wind variance observed at the MU radar could be explained by a gravity wave model, although they did not compare their observations with any other models, such as a model of stratified turbulence. Further, Doppler shifting effects of the observed variance spectrum, such as those discussed by VanZandt et al. (1990), can lead to complicated changes in the observed variances and it is beyond the scope of this study to investigate such effects.

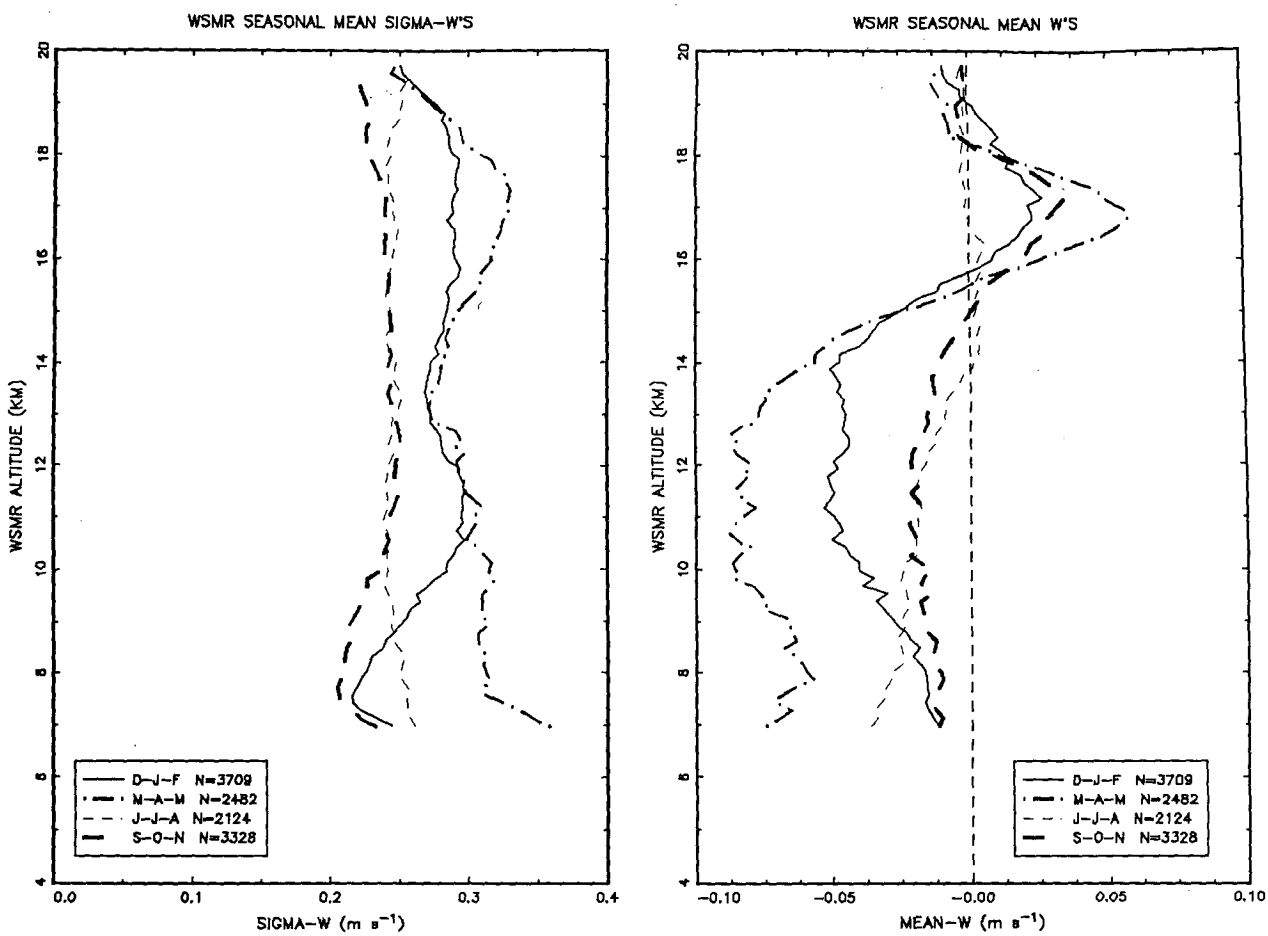

FIG. 8. Seasonal mean vertical velocity (right) and the standard deviation of vertical velocity over 1-h periods (left).

b. Vertical velocity

The variance of the vertical velocity, σ_w^2, is often taken as an indicator of gravity wave amplitude. Figure 8 shows the mean profiles of σ_w and of the mean vertical velocity $\bar{w}$. Note that the mean σ_w is largest in winter and spring at all levels above about 8 km. The values for summer and fall are fairly uniform from 10 to nearly 20 km. Nastrom and Eaton (1993a) studied a period during the spring and noted that the peak in σ_w^2 seen near 17 km appears to be related to gravity wave growth and instability.

Values of $\bar{w}$ in Fig. 8 are downward at several centimeters per second below about 15 km and show a small region of upward motions in the lower stratosphere during all seasons. Nastrom and Gage (1984) also noted downward motions in the $\bar{w}$ at Poker Flat, Alaska, which is in a distinctly different climatic regime at relatively high latitude. Nastrom and VanZandt (1994) have presented a theory that predicts that the observed $\bar{w}$ will be downward when there is upward energy propagation by gravity waves. This effect arises from the nonuniform radar reflectivity perturbations in the gravity waves and the correlation between perturbation lapse rate and vertical velocity. They predict that the magnitude of $\bar{w}$ is proportional to the gravity wave amplitude, and thus is proportional to σ_w when σ_w is an indicator of gravity wave amplitude. Largest $\bar{w}$'s are observed during fall and winter in the troposphere in Fig. 8. Largest σ_w's are also seen during fall and winter, although the correlation between $\bar{w}$ and σ_w is not perfect. One reason that the correlation between $\bar{w}$ and σ_w is not perfect could be that the relative fractions of trapped and vertically propagating gravity waves may change with season, since trapped waves make no contribution to $\bar{w}$ in this theory but do add to σ_w.

c. C_N^2

Figure 9a shows profiles of the seasonal mean of $\log C_N^2$ for the beam in the east–west plane, the u beam. Within turbulent regions the values of C_N^2 are given by

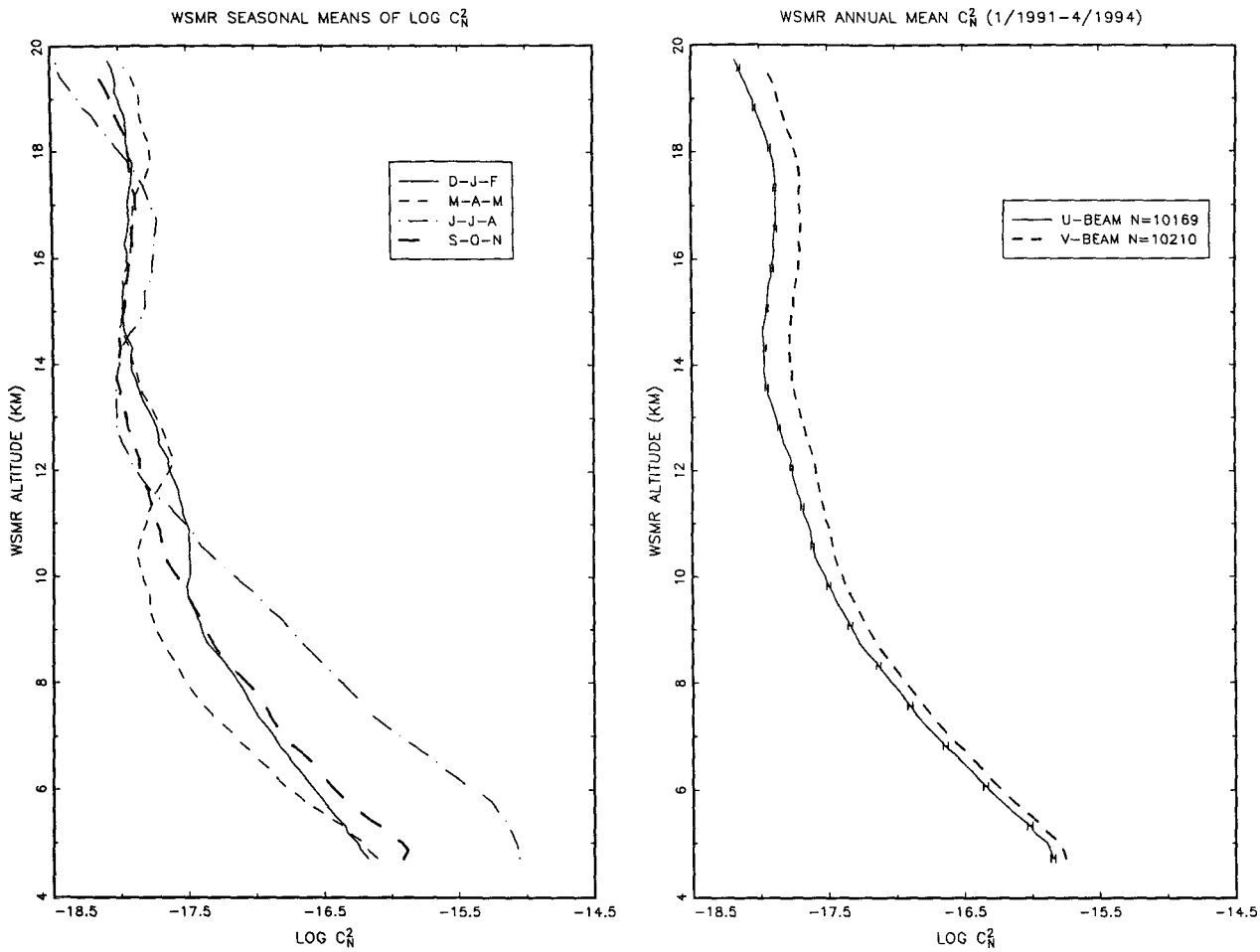

FIG. 9. Comparison of the (left) seasonal mean profiles of C_N^2 on the beam in the east–west plane, (right) annual mean profiles of C_N^2 on the east–west and north–south beams. In the right panel, error bars extend one standard error of the mean on either side of the mean.

$$C_N^2 = \alpha^2 \alpha' L_o^{4/3} M^2, \quad (1)$$

where a is a constant close to unity, α' is the ratio of the eddy diffusivities of heat and momentum and is taken to be near unity, L_o is the outer scale of the turbulence, and M^2 is the potential refractivity. Mean values of C_N^2 as seen by the radar depend on the fraction of the radar sample volume that is actively turbulent (Warnock and VanZandt 1985). Potential refractivity M^2 is proportional to the humidity, the vertical gradient of humidity, and the vertical gradient of temperature as well as the density of air and is given by

$$M^2 = \left(77 \times 10^{-6} \frac{P}{T\theta}\right)^2 \left[\frac{\partial \theta}{\partial z}\left(1 + \frac{15\,500q}{T}\right) - \frac{15\,500\theta}{2T}\frac{\partial q}{\partial z}\right]^2, \quad (2)$$

where the symbols have their usual meanings (Gage 1990). It is seen that in dry air M^2 will be proportional to the product of static stability and density; in such regions it thus decays with height proportional to density if there is constant static stability.

In Fig. 9a, largest values of $\log C_N^2$ are seen in the troposphere during summer and correlate with the regions of largest humidity. In the troposphere, the single largest contribution to the variability of M^2 comes from humidity gradients (Tsuda et al. 1988; Gage 1990). During the other seasons, and in the stratosphere, there is surprisingly relatively little variation of the mean C_N^2; this is likely because, as seen in Figs. 3 and 4, the mean wind shear (leading to local turbulence) is fairly constant with season and the mean static stability in the stratosphere does not change much with season. For example, the seasonal means of Brunt–Väisälä frequency squared at El Paso, about 50 km south of WSMR, in the layer from 150 to 100 mb are 3.76, 4.23, 4.02, and 3.75 $\times 10^{-4}$ s^{-2} for winter, spring, summer, and autumn, respectively.

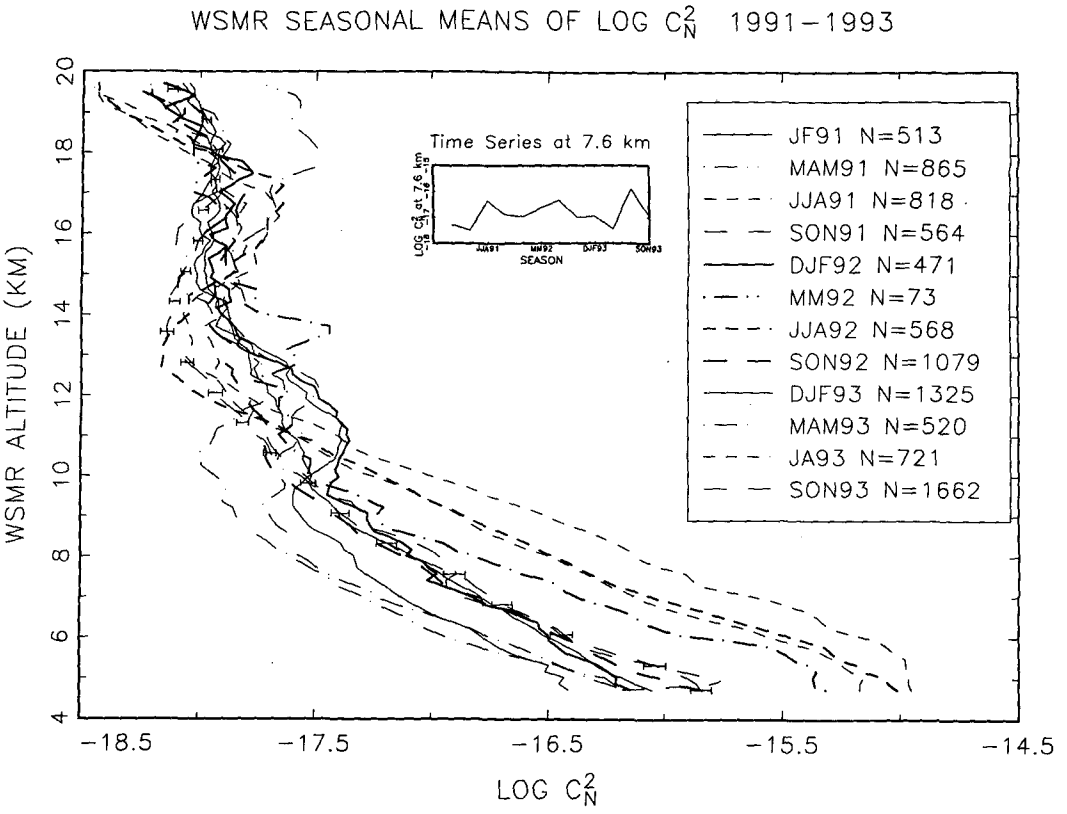

FIG. 10. Seasonal mean profiles of C_N^2 for 1991–93 at WSMR. Notice there is no obvious interannual trend. Here, N is the number of hourly means used at 7.6 km for each season; error bars are for autumn 1993 (SON93). The inset shows a time series at 7.6 km.

Figure 9b compares the annual mean profiles of $\log C_N^2$ for the east–west and north–south beams. The zonal beam's values are smaller, about 1 dB in the troposphere and about 2 dB in the stratosphere. Comparisons of mean profiles for individual seasons show differences similar to these annual mean results (Nastrom 1995). The reason for the difference between beams is not understood and may reflect a genuine atmospheric anisotropy in small-scale turbulence. The radar was operated with the oblique beams facing north and east until 25 March 1992, when the beams were changed to face south and west: reversing the pointing directions had no effect on the difference between the zonal and meridional beams. In Eq. (1), all factors including M^2 are expected to be isotropic, except L_o could be anisotropic. Mean values of the spectral width (not shown), which is directly related to small-scale turbulence intensity, are also larger on the north–south beam, suggesting an anisotropy in small-scale turbulence. Note that the pattern between the east and north beams in Fig. 9 is very different from that seen in Fig. 7, where comparisons of the temporal variances of the two beams show $\sigma_v^2 < \sigma_u^2$ in the stratosphere. This difference suggests that the small-scale turbulence and the temporal variations of the background flow do not arise from the same process.

Interannual variations of the seasonal means of $\log C_N^2$ are given in Fig. 10. The interseasonal variations seen in Fig. 10 are clearly much more important than the interannual variations for any given season. For example, in the troposphere the mean summer profiles are the largest values found during every year, and the values for spring and winter are the smallest. Variations among all seasons are relatively small in the stratosphere. Note that there is no apparent trend of C_N^2 with time at any height at WSMR, in contrast to the interannual trend in Colorado reported by Frisch et al. (1990).

4. Diurnal variations

We use the term "diurnal variation" to mean the 24-h cycle and all of its harmonics. To study the diurnal cycle, hourly means of wind speed, $\log C_N^2$, σ_w, and spectral width were sorted according to hour of the day during each season and the time series of the 24 hourly means were inspected for apparent diurnal cycles. For example, Fig. 11 shows the diurnal curves for beam 2,

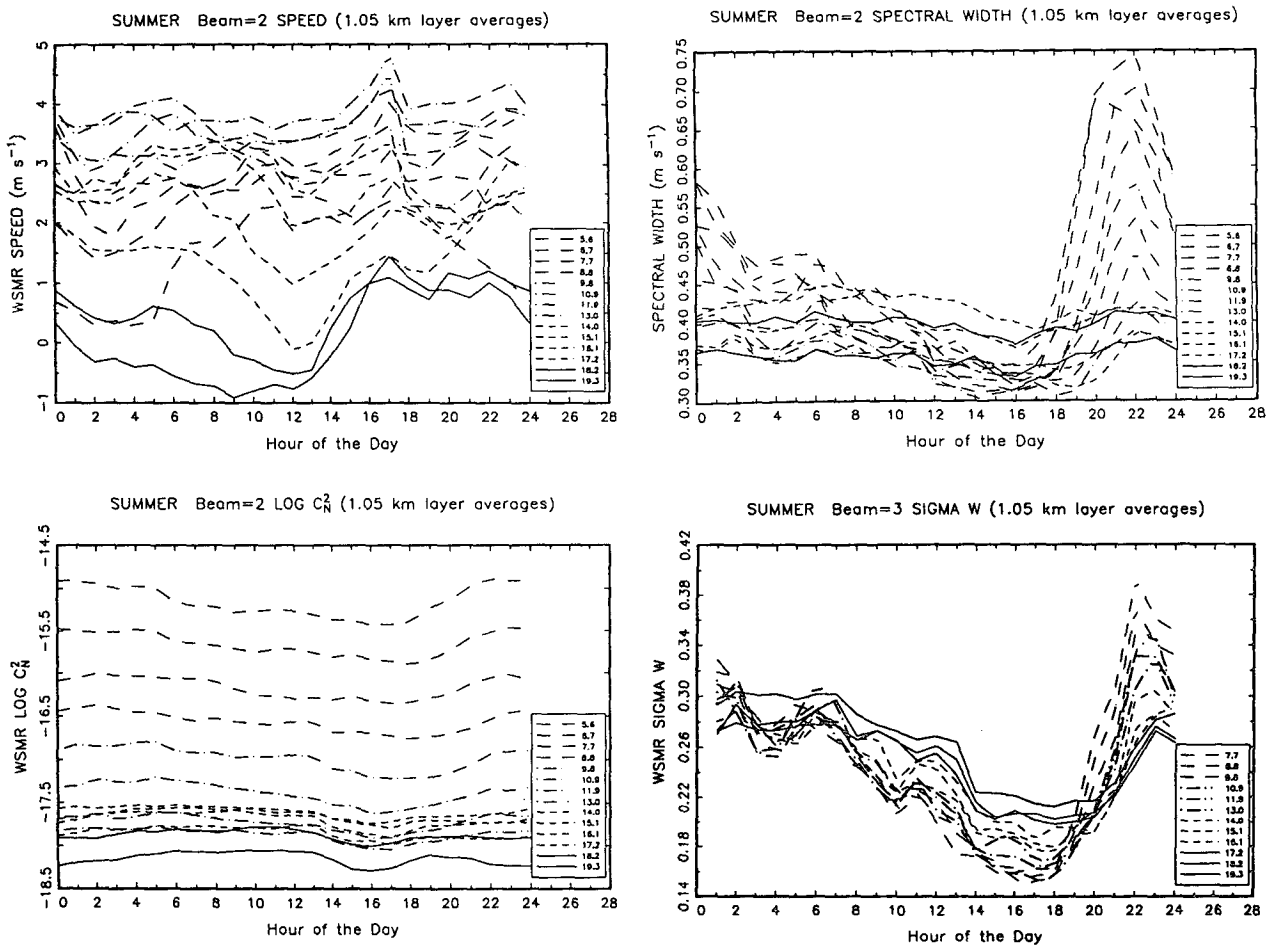

FIG. 11. Mean diurnal curves of the wind speed, spectral width, and C_N^2 on the beam in the north–south plane and of the standard deviation of the vertical velocity during summer.

in the meridional plane, during summer. The data are plotted as a function of UTC; local time at WSMR is 7 h behind UTC. In each panel, seven range gates have been averaged to give curves for layers 1.05 km deep. In the upper left panel, for wind speed, there is an apparent semidiurnal variation in the lower stratosphere, becoming more nearly diurnal at the upper levels shown. The diurnal cycle in wind speed sometimes is even stronger as shown in Table 2. Table 2 gives the amplitude and phase (time of maximum northward or eastward wind speed) of the diurnal and semidiurnal cycles, and the percent of the total daily variance explained by each cycle for each season. As pointed out by others (e.g., Wallace and Tadd 1974; May and Wilczak 1993), the diurnal tidal pattern in rough terrain is strongly influenced by the terrain. The large percentage of the total daily variance explained by the diurnal and semidiurnal cycles suggests that analyses that use only a few points each day, such as Wallace and Tadd, should give reasonable estimates. A detailed comparison of our results with predictions from tidal theory, such as the study by Williams et al. (1992), is beyond the scope of this study.

Doppler spectral width has a large afternoon maximum in the troposphere during summer. The afternoon maximum in the midtroposphere is about a factor of 2 larger than the morning minimum. The amplitude of the afternoon maximum decreases steadily with height throughout the troposphere and is very small in the stratosphere. The widths are given here as reported, without corrections for shear broadening, etc., as discussed by Hocking (1985), although the light winds during summer should reduce any such problems; certainly, the gross features of the diurnal cycle of width in Fig. 11 are correct. A detailed study of spectral widths at WSMR is underway and will be given in a separate paper.

Diurnal variations of $\log C_N^2$ are relatively small (Fig. 11). In the midtroposphere the maximum values are found in the afternoon and are about 5 dB larger than

TABLE 2. Amplitude (m s^{-1}), percent of explained variance (PEV), and phase (UTC hour of maximum wind) of the diurnal and semidiurnal oscillations in seasonal mean wind speed in the stratosphere at WSMR. For the semidiurnal oscillation, the phase is the time of first maximum.

		Zonal winds						Meridional winds					
		Amplitude		PEV		Phase		Amplitude		PEV		Phase	
	Alt	Diur	Semi	Diur	Semi	Diur	Semi	Diur	Semi	Diur	Semi	Diur	Semi
Winter	16.2	0.565	0.497	0.430	0.333	−3.96	−2.16	0.236	0.445	0.171	0.612	11.0	−3.06
Winter	17.2	0.171	0.244	0.123	0.251	3.67	0.0325	0.355	0.424	0.337	0.481	5.94	−3.33
Winter	18.3	0.938	0.221	0.857	0.0474	4.78	−1.70	0.542	0.343	0.683	0.273	−0.927	−3.80
Winter	19.3	0.618	0.418	0.611	0.280	−3.91	0.191	0.280	0.370	0.343	0.601	−11.1	−3.02
Spring	16.2	0.606	0.462	0.509	0.296	1.84	−1.47	0.298	0.515	0.219	0.653	−0.987	−4.07
Spring	17.2	0.452	0.502	0.402	0.494	−2.49	−0.657	0.101	0.425	0.043	0.772	−11.2	−3.14
Spring	18.3	0.330	0.761	0.150	0.794	−11.9	−0.276	0.331	0.613	0.21	0.737	1.45	−3.42
Spring	19.3	0.107	0.837	0.0157	0.951	−1.39	−0.267	0.147	0.670	0.041	0.863	4.69	−3.76
Summer	16.2	0.247	0.446	0.215	0.701	11.0	−1.07	0.560	0.362	0.615	0.258	2.09	−5.31
Summer	17.2	0.559	0.554	0.476	0.468	6.52	−1.35	0.851	0.191	0.810	0.041	0.377	−4.24
Summer	18.3	0.405	0.582	0.307	0.634	3.30	−1.88	0.631	0.284	0.704	0.142	−1.90	−4.91
Summer	19.3	0.953	0.449	0.777	0.172	2.24	−1.67	0.998	0.214	0.901	0.041	−3.17	−5.08
Fall	16.2	0.567	0.530	0.474	0.414	6.60	−0.948	1.04	0.522	0.769	0.195	0.550	−3.98
Fall	17.2	0.551	0.536	0.481	0.457	7.54	−1.14	0.735	0.560	0.615	0.357	−0.16	−4.21
Fall	18.3	0.387	0.489	0.346	0.555	2.92	−0.768	0.818	0.460	0.714	0.225	−3.01	−4.46
Fall	19.3	0.481	0.523	0.439	0.520	−1.22	−0.853	0.486	0.489	0.476	0.481	−5.60	−4.03

morning values. The time of maximum occurs later with increasing height and at 12 km it occurs near local midnight. The progression of the time of maximum with height in the troposphere is likely related to the upward flux of moisture with the onset of afternoon convection. In the lower stratosphere the daily range of values is only a few decibels, with the daily maximum found near 1000 UTC. These results are similar to Nastrom et al. (1985), who found diurnal ranges of 5–8 dB over Colorado and Alaska and noted a phase reversal between the troposphere and the stratosphere. At the very highest altitudes shown in Fig. 11, there is a semidiurnal cycle. Questions concerning the magnitude of the diurnal variation of C_N^2 in the stratosphere arose during a one-week intercomparison study involving the Flatland VHF radar, optical devices, and thermosondes (Eaton et al. 1989). Now, from the analysis of the long-term continuous measurements presented here we have a more reliable climatological estimate of the diurnal variations of C_N^2 at 6–20 km over WSMR.

The diurnal cycle in σ_w shows a strong afternoon maximum at all altitudes. The time of maximum is about an hour later in the stratosphere than in the troposphere. The daily range is about a factor of 2.1 near 8 km and decreases to about a factor of 1.3 near 19 km. The daily ranges during other seasons are generally smaller and more uniform with height as shown in Fig. 12. Clearly, the general form of the diurnal variation in σ_w does not change much with height in a given season (ignoring the apparent instrumental effects at the lowest altitudes during fall and winter). Sato (1990, 1992) has discussed the diurnal changes in vertical wind variability at the MU radar in Japan and notes that the afternoon maximum in the troposphere is likely due to convective activity. Ecklund and Balsley (1981) have also noted an afternoon maximum in σ_w and a correlation of σ_w with afternoon convection at the Platteville radar in Colorado.

5. Summary and conclusions

A very large and unique dataset has been collected with the 50-MHz profiler at WSMR. The available data span the period January 1991–April 1994 and cover the height range from about 6 to 20 km with 150-m vertical resolution and 3-min time resolution. About 90% of the available data during the 12 251 h of observations survived quality control checks at all altitudes. This dataset is suitable for climatological studies of atmospheric variables such as wind speed, vertical wind variability, and indicators of small-scale turbulence such as spectral width and C_N^2. This paper has emphasized the seasonal, interannual, and diurnal changes of these variables.

The following conclusions have been reached:

1) The radar observations reach into the stratospheric summer easterlies above 17 km. During all other seasons and levels the mean zonal winds are from the west. Mean meridional winds are from the south at all times except during fall and, above 17 km, during

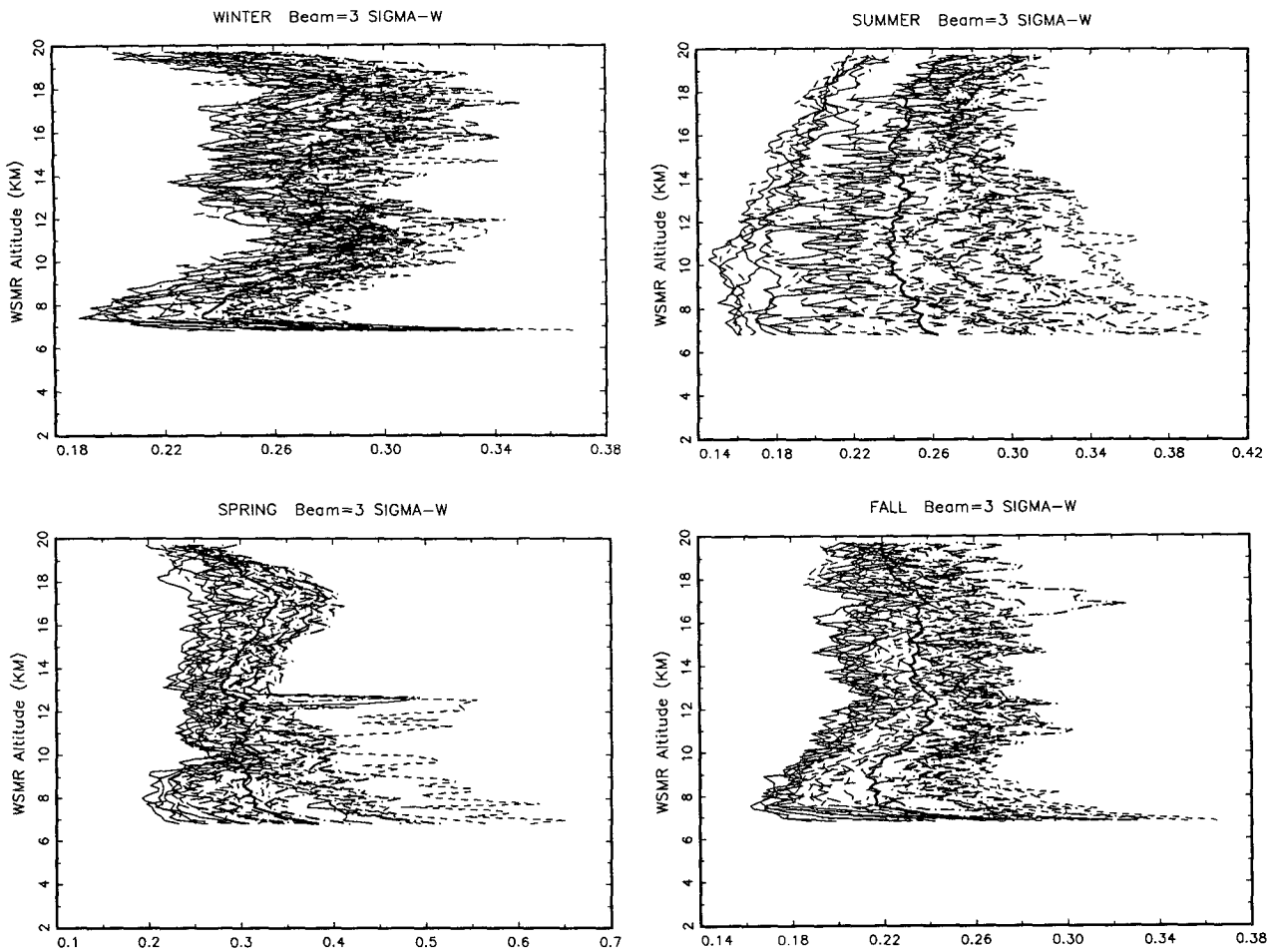

FIG. 12. Vertical profiles of the mean σ_W sorted by hour of the day for each season. Successive 6-h periods have different line types. The mean over 24 h is shown by a bold line in each panel.

winter. The maximum mean meridional winds are found during summer.

2) The seasonal mean vertical wind shear is a maximum near 12 km during winter and spring. The seasonal mean values are very similar in the stratosphere and, except during summer, in the midtroposphere.

3) The variances of all three wind components, computed over 1-h periods, follow a lognormal frequency distribution.

4) Largest mean variance of all three components of the winds are found near 16 km in spring and the smallest are found near 8 km in the fall.

5) The variances of the horizontal winds are anisotropic, with the meridional wind variance larger in the troposphere during fall through spring, and the zonal wind variance larger in the stratosphere during winter and spring. During summer the variances of the horizontal winds are nearly equal at all heights below about 17 km.

6) The mean vertical velocity is downward in the troposphere, with largest values over 5 cm s^{-1} during winter and spring, and is slightly upward in the lower stratosphere. There is a rough correlation between σ_w and $\bar{w}$.

7) The mean $\log C_N^2$ is largest in the troposphere in summer; presumably due to increased water vapor there then. There is very little seasonal change of mean $\log C_N^2$ in the stratosphere.

8) There is no evidence of an interannual trend of mean C_N^2 at WSMR.

9) At WSMR, there is a strong diurnal cycle of wind speed in the stratosphere, with evidence of a semidiurnal component as well. The spectral width has largest diurnal changes in the troposphere during summer, with a daily range of over a factor of 2 during summer. The diurnal cycle of mean C_N^2 is also largest in the troposphere, with a daily range during summer of about 5 dB.

10) The daily cycle of the hourly variance of vertical velocity (an indicator of gravity wave activity) is largest during summer when it shows a slight decrease with altitude. During other seasons the daily range of σ_w is relatively uniform with altitude.

Acknowledgments. Steve Smith of NASA gave many useful comments on an early version of this paper.

REFERENCES

Balsley, B. B., W. L. Ecklund, D. A. Carter, and P. E. Johnston, 1979: The Poker Flat MST radar: First results. *Geophys. Res. Lett.*, **6,** 921–924.

Eaton, F., and Coauthors, 1989: Comparisons of the transverse coherence length and isoplanatic angle from measurements taken with the Flatland very high frequency radar, optical techniques, and thermosondes. *Proc. of SPIE,* Los Angles, CA, Soc. Photo-Opt. Instrum. Eng., 130–138.

——, S. A. McLaughlin, and J. R. Hines, 1995: A new FM-CW radar for studying planetary boundary layer morphology. *Radio Sci.*, **30,** 75–88.

Ecklund, W. L., and B. B. Balsley, 1981: A comparison of vertical wind variability observed with the Platteville VHF radar and local weather conditions. Preprints, *20th Conf. on Radar Meteorology,* Boston, MA, Amer. Meteor. Soc., 104–109.

Frisch, A. S., B. L. Weber, D. B. Wuertz, R. G. Strauch, and D. A. Merritt, 1990: The variations of C_N^2 between 4 and 18 km above sea level as measured over 5 years. *J. Appl. Meteor.*, **29,** 645–651.

Gage, K. S., 1990: Radar observations of the free atmosphere: Structure and dynamics. *Radar in Meteorology,* David Atlas, Ed., Amer. Meteor. Soc., 534–565.

Hines, J. R., S. A. McLaughlin, F. D. Eaton, and W. H. Hatch, 1993: The US Army Atmospheric Profiler Research Facility: Introduction and capabilities. Preprints, *Eighth Symp. on Meteorological Observations and Instrumentation,* Anaheim, CA, Amer. Meteor. Soc., 237–242.

Hocking, W. K., 1985: Measurement of turbulent energy dissipation rates in the middle atmosphere by radar techniques: A review. *Radio Sci.*, **20,** 1403–1422.

Hoidale, M. M., M. P. Dayton, and L. Newman, 1975: Atmospheric Structure, White Sands Missile Range, New Mexico, Part 3, Upper Air and Surface Data: Holloman Site. ECOM-DR-877, US Army, White Sands Missile Range, NM, 240 pp.

Kato, S., T. Tsuda, M. Yamamoto, T. Sato, and S. Fukao, 1986: First results obtained with a middle and upper atmosphere (MU) radar. *J. Atmos. Terr. Phys.*, **48,** 1259–1267.

May, P. T., and J. M. Wilczak, 1993: Diurnal and seasonal variations of boundary-layer structure observed with a radar wind profiler and RASS. *Mon. Wea. Rev.*, **121,** 673–682.

Nastrom, G. D., 1995: Variability of C_N^2 and wind as seen by the 50 MHz radar at White Sands Missile Range, NM. ARL-CR-197, White Sands Missile Range, NM, 54 pp.

——, and K. S. Gage, 1984: A brief climatology of vertical wind variability in the troposphere and stratosphere as seen by the Poker Flat, Alaska, MST radar. *J. Climate Appl. Meteor.*, **23,** 453–460.

——, and F. D. Eaton, 1993a: The coupling of gravity waves and turbulence at White Sands, New Mexico, from VHF radar observations. *J. Appl. Meteor.*, **32,** 81–87.

——, and ——, 1993b: The onset of the summer monsoon over White Sands Missile Range, New Mexico, as seen by VHF radar. *J. Geophys. Res.*, **98,** 23 235–23 243.

——, and T. E. VanZandt, 1994: Mean vertical motions seen by radar wind profilers. *J. Appl. Meteor.*, **33,** 984–995.

——, W. L. Ecklund, K. S. Gage, and R. G. Strauch, 1985: The diurnal variation of backscattered power from VHF Doppler radar measurements in Colorado and Alaska. *Radio Sci.*, **20,** 1509–1517.

Ruster, R., J. Klostermeyer, and J. Rottger, 1986: SOUSY VHF radar measurements in the lower and middle atmosphere. *IEEE Trans. Geosci. Remote Sens.*, GE-**24,** 966–974.

Sato, K., 1990: Vertical wind disturbances in the troposphere and lower stratosphere observed by the MU radar. *J. Atmos. Sci.*, **47,** 2803–2817.

——, 1992: Vertical wind disturbances in the afternoon of mid-summer revealed by the MU radar. *Geophys. Res. Lett.*, **19,** 1943–1946.

Tsuda, T., P. T. May, T. Sato, S. Kato, and S. Fukao, 1988: Simultaneous observations of reflection echoes and refractive index gradient in the troposphere and lower stratosphere. *Radio Sci.*, **23,** 655–665.

VanZandt, T. E., S. A. Smith, T. Tsuda, D. C. Fritts, T. Sato, S. Fukao, and S. Kato, 1990: Studies of velocity fluctuations in the lower atmosphere using the MU radar. Part I: Azimuthal anisotropy. *J. Atmos. Sci.*, **47,** 39–50.

Wallace, J. M., and R. F. Tadd, 1974: Some further results concerning the vertical structure of atmospheric tidal motions within the lowest 30 kilometers. *Mon. Wea. Rev.*, **102,** 795–803.

Warnock, J. M., and T. E. VanZandt, 1985: A statistical model to estimate the refractivity turbulence structure constant C_N^2 in the free atmosphere. NOAA TM-ERL-AL-10, 175 pp.

Weber, B. L., and Coauthors, 1990: Preliminary evaluation of the first NOAA demonstration network wind profiler. *J. Atmos. Oceanic Technol.*, **7,** 909–918.

Wilfong, T. L., S. A. Smith, and R. L. Creasy, 1993: High temporal resolution velocity estimates from a wind profiler. *Spacecr. Rockets,* **30,** 348–354.

Williams, C. R., S. K. Avery, J. R. McAfee, and K. S. Gage, 1992: Comparison of observed diurnal and semidiurnal tropospheric winds at Christmas Island with tidal theory. *Geophys. Res. Lett.*, **19,** 1471–1474.